Photoinduced Barkhausen Effect in the Ferromagnetic Semiconductor (Ga,Mn)As

G. V. Astakhov,* J. Schwittek, G. M. Schott, C. Gould, W. Ossau, K. Brunner, and L. W. Molenkamp

Physikalisches Institut (EP3), Universität Würzburg, 97074 Würzburg, Germany

(Received 16 June 2010; published 18 January 2011)

Magnetization of ferromagnetic materials commonly occurs via random jumps of domain walls between pinning sites, a phenomenon known as the Barkhausen effect. Using strongly focused light pulses of appropriate power and duration we demonstrate the ability to selectively activate single jumps in the domain wall propagation in (Ga,Mn)As, manifesting itself as a discrete photoinduced domain wall creep as a function of illumination time. The propagation velocity can be increased over 7 orders of magnitude varying the illumination power density and the magnetic field.

DOI: 10.1103/PhysRevLett.106.037204 PACS numbers: 75.60.−d, 75.50.Pp, 78.20.Ls

Many magnetic recording technologies make use of the natural tendency of ferromagnetic materials to fragment into domains with different magnetization orientations, separated by domain walls (DWs) [1–4]. These DWs can move, driven either by external magnetic field or by spin polarized current [1–9], which is the conceptual basis for various magnetic storage and logic devices. For applications, it is essential to have adjustable and repeatable control over DW motion, which is directly linked to the DW pinning and depinning processes in the ferromagnetic material. Strong pinning prevents thermal fluctuations of the magnetization, whereas weak pinning is needed to allow for low power and high speed recording. This implies that long-term storage media and efficient recording procedures have opposite requirements for the pinning strength. Pinning sites with desired properties can be introduced during the fabrication process; however, their pinning strength remains unchanged whenever the device is in use. From this perspective, realizing DW pinning sites of adjustable strength represents an important step forward for magnetic recording techniques.

Here, we demonstrate, using Kerr microscopy as a function of illumination time, the ability to selectively address single DW pinning sites and to switch them between pinning and depinning configurations. This forces propagation of the DWs via controllable photoactivated jumps, which result in discrete increases of the domain area. We find that the time between such light-induced Barkhausen jumps (which determines the DW propagation velocity) exponentially decreases with light intensity.

We perform our experiments on the ferromagnetic semiconductor (Ga,Mn)As, which, because of its reduced magnetization and intermediate carrier density, is frequently used as a demonstrator material exploring novel device concepts [10,11]. The ferromagnetic coupling between Mn ions in the GaAs semiconductor host is mediated by itinerant holes [12]. Here, we present results for a $Ga_{0.99}Mn_{0.01}As$ layer, $l = 0.36$ μm thick, grown by low-temperature (LT) molecular beam epitaxy [13] on a (001)-oriented GaAs substrate and LT-GaAs buffer. The sample shows a clear perpendicular-to-plane easy axis of magnetization and a Curie temperature $T_C = 25$ K. Magnetization measurements with a SQUID reveal an average concentration $x \approx 0.005$ of magnetically active ions. The sample is insulating at low temperatures, indicating partial compensation of p-type doping due to the presence of interstitial Mn defects.

The local magnetization M of the sample is measured by means of the magneto-optical Kerr effect. The linearly polarized light of a solid state laser (635 nm) is reflected from the sample surface, and the angle of the Kerr rotation $\theta \propto M$ is detected by a balanced photodiode scheme. All measurements are performed at $T = 2$ K, with the sample immersed in superfluid helium. We found that in this sample the coercive field H_c drops rapidly with the laser power P from the ''dark'' value $H_{cd} = 525$ Oe to the ''light'' value $H_{cl} = 100$ Oe. This is the so-called photocoercivity effect (PCE) [14,15] that we have previously demonstrated to occur in low-doped (Ga,Mn)As. We emphasize that the PCE is of nonthermal origin, as evidenced by the temperature and power dependencies of the coercivity and magnetization, and by observations of the effect at low power densities where lattice heating can be neglected [14,16].

In order to measure magnetization with good spatial resolution, we use an optical objective [numerical aperture (NA) = 0.42) mounted on a piezosystem. The objective focuses the laser beam to a circular spot, and its shape and size are monitored *in situ* during all experiments using a charge-coupled device (CCD) [Fig. 1(a)]. A line cut through the focused laser spot is well described by a Gaussian distribution, $I(r) = I_0 \exp(-\frac{r^2}{\Delta^2})$ with $\Delta = 1.2$ μm.

We now use the PCE to create magnetic domains [14]. First, the magnetic layer is uniformly magnetized by applying a strong magnetic field. Then, a reversed bias magnetic field H_0, such that $H_{cd} > H_0 > H_{cl}$, is applied. The sample is illuminated by the focused laser during time τ, and then the magnetic field is switched off. A magnetic domain created after a $\tau = 60$ s long illumination is shown

in Fig. 1(b). The important point to note is that it is significantly larger than the laser spot [compare to Fig. 1(a)].

Figure 1(c) shows the diameter S of several optically created magnetic domains as a function of illumination time τ (circles). The error bars in the figure correspond to the deviations of the domain shape from a circle. We find that the dependence $S(\tau)$ correlates with the size of the laser spot. When Δ is increased from $\Delta_1 = 1.2$ μm to $\Delta_2 = 4.5$ μm, while the power density in the center of the laser spot $I_0 = \frac{P}{\pi\Delta^2}$ is kept constant, the domain size increases approximately by the same proportion for each τ, i.e., $S_1(\tau)/S_2(\tau) \approx \Delta_1/\Delta_2$ [triangles in Fig. 1(c)].

We now discuss possible microscopic mechanisms for the growth of the photoinduced magnetic domains. At first glance, one expects that the data of Fig. 1(c) can be explained by field-driven DW motion of the nucleated domains [6–9]. However, this mechanism can be ruled out by our observation that in the dark and in low magnetic fields $H_0 < H_{cd}$ the magnetic domains do not change in size.

In order to explain the experimental data of Fig. 1(c) we propose the occurrence of photoinduced DW creep, as schematically shown in Figs. 2(a)–2(c). Consider the pinned DW of a nucleated domain [Fig. 2(a)]. In low concentration (Ga,Mn)As, a likely origin of DW pinning is the inhomogeneous distribution of interstitial Mn_I defects, which compensate the p-type doping provided by substitutional Mn_{Ga} acceptors [17]. These defects can form insulating nanoislands [18], which act as photosensitive DW pinning sites. Because of the band bending in the vicinity of such islands, the photocreated carriers are separated: the photoelectrons are accumulated on ionized Mn_I donors [19], while the photoholes move towards the conducting regions and screen the DW pinning sites. This corresponds to process (A) indicated by the red arrow in Fig. 2(a). Uniform illumination of these pinning sites results in the PCE [14].

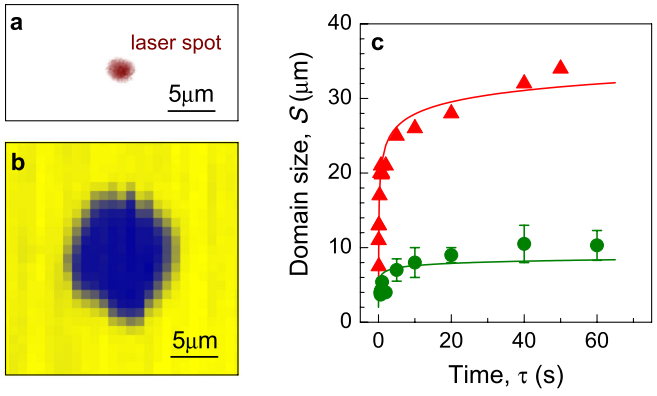

FIG. 1 (color online). (a) A CCD image of the focused laser beam. (b) A magnetic domain created at $H_0 = 350$ Oe by an optical pulse with $P = 14$ μW and $\tau = 60$ s. (c) Diameter S of a magnetic domain created at $H_0 = 350$ Oe as a function of illumination time τ: circles, $\Delta = 1.2$ μm and $P = 14$ μW; triangles, $\Delta = 4.5$ μm and $P = 140$ μW. The solid lines are fits to Eq. (1) with $\tau_0 = 2$ ms.

However, the intensity distribution of the focused laser beam is not uniform. In Fig. 2(b) and 2(c), the intensity profile at the edge of the laser spot is schematically represented by the background gray tone. When the local intensity $I(r)$ is low, the accumulation of photocarriers occurs slowly and the time τ_A required to depin the DW increases [Fig. 2(b)]. Depinned DWs move to the next pinning site, driven by the magnetic field. This process (B) is indicated by the green arrow in Fig. 2(c).

In the limit that $\tau_A \gg \tau_B$, the DW creep occurs via discrete photoinduced jumps between pinning sites, resulting in a stepwise increase of the domain size δS. The time between these jumps is determined by the process (A) and we use the simplest approximation $\tau_A \propto 1/I(r)$. For long illumination times, when δS much smaller than the domain size S, the DW creep can be considered as a quasicontinuous process. Applying then $\tau \propto 1/I(S)$, one obtains

$$S = 2\Delta\sqrt{\ln\frac{\tau}{\tau_0}}. \quad (1)$$

This behavior is exactly what is observed experimentally in Fig. 1(c) (we will show below that we indeed have

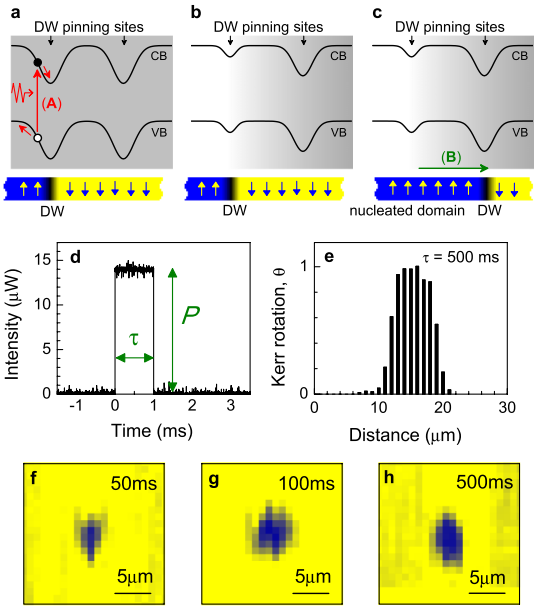

FIG. 2 (color online). (a)–(c) Schematic illustrations of the photoinduced Barkhausen effect. The processes (A) and (B) discussed in the main text are indicated by arrows. CB (VB) stands for conduction (valence) band. (d) A rectangularly shaped pulse with $P = 14$ μW and $\tau = 1$ ms as recorded using a photodiode and a storage oscilloscope. (e) Cross section of a magnetic domain. The y axis is scaled such that 0 and 1 correspond to the Kerr angles obtained for the layer uniformly magnetized downwards and upwards, respectively. (f)–(h) Magnetic domains created at $H_0 = 350$ Oe by the optical pulses with $P = 14$ μW and $\tau = 50$, 100, and 500 ms, respectively.

$\tau_A \gg \tau_B$ in this experiment). The drawn lines in Fig. 1(c) are fits to Eq. (1) with τ_0 as fitting parameter. The physical meaning of τ_0 is that it represents the minimum illumination time required to depin a DW in the center of the laser spot ($S = 0$). Experimentally, we find that τ_0 depends strongly on excitation power density I_0.

So far, we have concentrated on large magnetic domains $S \gg \Delta$. However, in order to resolve individual photoinduced DW jumps it is necessary to study the temporal evolution of small magnetic domains. For these purposes we use a pulse generator to a solid state laser. An example of a rectangle-shaped optical pulse with $P = 14$ μW and $\tau = 1$ ms is shown in Fig. 2(d).

Magnetic domains created by such rectangular pulses with $\tau = 50$, 100, and 500 ms are shown in Figs. 2(f)–2(h), respectively. They have irregular shapes not described by Eq. (1), which implicitly assumes radial symmetry. Therefore, we analyze the area A of these magnetic domains obtained from 2D scans defined as

$$A = \sum \theta_{x,y} \delta_x \delta_y. \tag{2}$$

Here, $\theta_{x,y}$ is the Kerr rotation at a point with coordinates (x, y) and δ_x, $\delta_y = 1$ μm are scanning steps along x and y directions. The Kerr rotation in Eq. (2) is calibrated such that 0 and 1 correspond to the layer uniformly magnetized downwards and upwards, respectively [Fig. 2(e)]. First, we analyze the area distribution of magnetic domains created at nominally the same conditions. Figure 3(a) shows A for different experiments with $\tau = 50$ ms. The error bars in Fig. 3 are due to a slight drift of the signal background during the spatial scans. Using these data we find the average area $A_2 = (19.5 \pm 1.9)$ μm^2 (the meaning of the suffix will become clear shortly). The standard deviation $\sigma_2 = 1.9$ μm^2 can be ascribed to statistical fluctuations in the position and pinning efficiency of the DW pinning sites. The normal distribution of experimentally obtained areas A

$$P_n(A) = \frac{1}{\sqrt{2\pi}\sigma_n} \exp\left(-\frac{(A - A_n)^2}{2\sigma_n^2}\right) \tag{3}$$

is indicated by the intensity of the background color in Fig. 3(a) with A_n and σ_n thus obtained (here, $n = 2$).

Figure 3(b) shows evolution of the domain area A as a function of illumination time. The area increases stepwise from the value A_2 of Fig. 3(a) to a larger value A_3 for $\tau \geq 100$ ms and remains—within error bars—constant up to $\tau = 700$ ms. The average value found from these data points is $A_3 = 28.4$ μm^2. Assuming that the standard deviation is $\sigma \propto \sqrt{A}$, we use $\sigma_3 = \sigma_2\sqrt{A_3/A_2}$ and obtain $\sigma_3 = 2.3$ μm^2. The normal distributions of Eq. (3) with obtained A_3 (A_2) and σ_3 (σ_2) are again indicated by the intensity of the background color in Fig. 3(b).

By varying the laser pulse length τ, we have resolved five discrete steps in the increase of domain area as a function of illumination time [Fig. 3(c)]. The steps are equidistant so that $A_n = nA_1$, where n is the step number and $A_1 = 9.75$ μm^2 [inset of Fig. 3(c)]. This observation points at the DW propagation occurring via photoactivated jumps between pinning sites, as explained in Figs. 2(a)–2(c). We emphasize that this propagation mechanism is deterministic and thus qualitatively different from the so-called Barkhausen avalanche, which is triggered by random fluctuations and characterized by a power-law behavior with respect to the jump size.

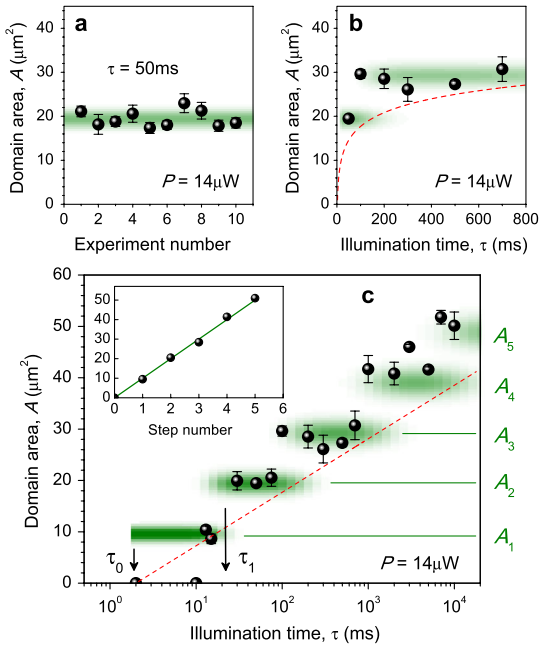

FIG. 3 (color online). (a) Area of several magnetic domains created under nominally the same conditions, with $\tau = 50$ ms. (b) Area of the magnetic domains as a function of the illumination time τ. (c) Photoinduced Barkhausen jumps as a function of the illumination time τ. Inset: Average area of magnetic domains A_n as a function of step number n. The dashed curves in (b) and (c) indicate the domain area predicted by Eq. (1). The background color in all panels corresponds to the probability density to create domain of area A (see text for details).

We now model the experimental data presented in Fig. 3(c). First, we plot the domain area A predicted by Eq. (1), i.e., $A(\tau) = \pi\Delta^2 \ln\tau/\tau_0$, as shown by the dashed curve in Fig. 3(c). At time τ_0, the magnetic domain is nucleated by starting the illumination. Subsequently, the domain grows until it reaches the first pinning site. On prolonged illumination, the domain area remains constant until $\tau_1 = \tau_0 \exp(\frac{A_1}{\pi\Delta^2})$, when the first pinning site is switched off, and the DW jumps to the next pinning site. Combining Eqs. (1) and (3), one finds for the probability that at time τ the nth pinning site is turned off the following expression:

$$\rho_n(\tau) = \frac{1}{2}\left[1 + \mathrm{erf}\left(\frac{A(\tau) - A_n}{\sqrt{2}\sigma_n}\right)\right], \tag{4}$$

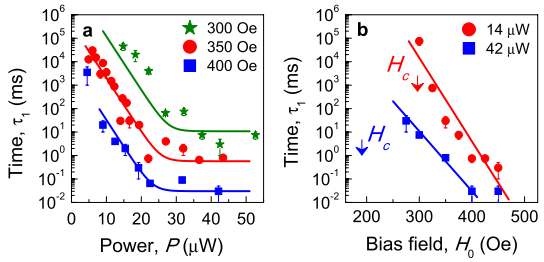

FIG. 4 (color online). Dynamics of the photoinduced DW propagation. (a) Characteristic time τ_1 as a function of laser power P for different external fields H_0. (b) Characteristic time τ_1 as a function of external field H_0 for different powers P. Solid lines in (a) and (b) are fits to Eq. (5) with $T = 1.1 \times 10^{15}$ s and $t = 20$ ns.

where $\sigma_n = \sqrt{n}\sigma_1$ and erf$(\cdot)$ denotes the error function. The probability for the nth jump of the DW, given by $\rho_{n-1}(1 - \rho_n)$, is indicated by the intensity of the background color in Fig. 3(c), and clearly found to be in quantitative agreement with the experimental data.

The dynamics of the photoinduced DW propagation is determined by which process is slowest, either DW depinning (with characteristic time τ_A) or DW propagation (characteristic time τ_B). Only τ_A should change with excitation power P and, therefore, these two processes can be distinguished by varying P. We concentrate on the characteristic time τ_1 required to induce the second Barkhausen jump [see Fig. 3(c)]. Figure 4(a) shows τ_1 as a function of P when domains are created at different magnetic fields H_0. The first thing to note is the extreme sensitivity of τ_1 to laser power: it changes more than 7 orders of magnitude when P is varied between 5 and 50 μW. Furthermore, while τ_1 decreases exponentially with P for low powers, it is nearly independent of P at high illumination power levels. We interpret this behavior as follows. For low powers the depinning process is slow compared to the DW propagation ($\tau_A \gg \tau_B$) and hence $\tau_1 \approx \tau_A$. With increasing P, the DW depinning speeds up according to $\tau_A \propto \exp(-P/P_A)$, where $P_A = 1.9$ μW is independent of H_0. For high powers $\tau_A \ll \tau_B$, and hence $\tau_1 \approx \tau_B$ is independent of P.

Figure 4(b) shows that τ_1 decreases as a function of magnetic field H_0. At $P = 14$ μW, when $\tau_1 \approx \tau_A$, the decrease must be due to a lowering of the DW pinning barrier. At $P = 42$ μW, when $\tau_1 \approx \tau_B$, the decrease can be explained by an increase of the DW propagation velocity with field [8]. The characteristic time τ_1 in the given ranges of P and H_0 is well described by the following empirical equation [cf. the solid lines in Figs. 4(a) and 4(b)]:

$$\tau_1 = T \exp\left(-\frac{P}{P_A} - \frac{H_0}{H_A}\right) + t \exp\left(\frac{H_{cd} - H_0}{H_B}\right). \quad (5)$$

The first term in Eq. (5) is an Arrhenius-type activation and assumes that the DW pinning barrier decreases linearly with P. The parameter T corresponds to the domain stability (thermal activation time) in the dark and in zero magnetic field. The second term describes field-driven DW propagation between pinning sites.

In conclusion, we have investigated light-induced DW propagation in the ferromagnetic semiconductor (Ga,Mn)As in an external magnetic field. We have found that this propagation occurs via photoactivated single jumps. This behavior is caused by the presence of DW pinning sites whose pinning efficiency decreases under optical illumination. Such a concept can be applied to room temperature recording media consisting of magnetically soft clusters coupled to a magnetically hard layer [20]. Clusters of diluted magnetic semiconductors can serve as programmable DW pinning sites, controlling the remagnetization processes in the hard layer.

The authors thank T. Kiessling for valuable discussions. The research leading to these results has received funding from the European Community's Seventh Framework Programme (FP7/2007-2013) under Grant No. NMP3-SL-2008-214469 (Ultramagnetron). G. V. A. acknowledges support from the DFG (Grant No. AS 310/2-1).

*Also at: A. F. Ioffe Physico-Technical Institute, RAS, 194021 St. Petersburg, Russia.
astakhov@physik.uni-wuerzburg.de

[1] M. Mansuripur, *The Physical Principles of Magneto-Optical Recording* (Cambridge University Press, Cambridge, England, 1995).
[2] S. Tsunashima, J. Phys. D **34**, R87 (2001).
[3] C. Chappert, A. Fert, and F. N. van Dau, Nature Mater. **6**, 813 (2007).
[4] S. S. P. Parkin, M. Hayashi, and L. Thomas, Science **320**, 190 (2008).
[5] S. Lemerle *et al.*, Phys. Rev. Lett. **80**, 849 (1998).
[6] L. Thevenard *et al.*, Phys. Rev. B **73**, 195331 (2006).
[7] M. Yamanouchi *et al.*, Science **317**, 1726 (2007).
[8] A. Dourlat *et al.*, Phys. Rev. B **78**, 161303(R) (2008).
[9] H. X. Tang *et al.*, Phys. Rev. B **74**, 041310(R) (2006).
[10] K. Pappert *et al.*, Nature Phys. **3**, 573 (2007).
[11] G. V. Astakhov *et al.*, Appl. Phys. Lett. **86**, 152506 (2005).
[12] H. Ohno, Science **281**, 951 (1998).
[13] G. M. Schott, W. Faschinger, and L. W. Molenkamp, Appl. Phys. Lett. **79**, 1807 (2001).
[14] G. V. Astakhov *et al.*, Phys. Rev. Lett. **102**, 187401 (2009).
[15] V. L. Korenev, Semicond. Sci. Technol. **23**, 114012 (2008).
[16] A. H. M. Reid *et al.*, Appl. Phys. Lett. **97**, 232503 (2010).
[17] K. Y. Wang *et al.*, J. Appl. Phys. **101**, 106101 (2007).
[18] D. M. Wang *et al.*, Phys. Rev. Lett. **102**, 256401 (2009).
[19] G. V. Astakhov *et al.*, Phys. Rev. Lett. **101**, 076602 (2008).
[20] R. Skomski *et al.*, IEEE Trans. Magn. **43**, 2163 (2007).